



Palaeoenvironmental changes after the Messinian Salinity Crisis in the Mediterranean Almeria-Nijar Basin (SE Spain) recorded by benthicforaminifera

Jose N. Perez-Asensio, Francisco J. Rodriguez-Tovar, Weronika Laska, Alfred Uchman

► To cite this version:

Jose N. Perez-Asensio, Francisco J. Rodriguez-Tovar, Weronika Laska, Alfred Uchman. Palaeoenvironmental changes after the Messinian Salinity Crisis in the Mediterranean Almeria-Nijar Basin (SE Spain) recorded by benthicforaminifera. *PALAEOGEOGRAPHY PALAEOLIMATOLOGY PALAEOECOLOGY*, 2021, 577, pp.110536. 10.1016/j.palaeo.2021.110536 . hal-03662536

HAL Id: hal-03662536

<https://hal.science/hal-03662536v1>

Submitted on 2 Aug 2023

HAL is a multi-disciplinary open access archive for the deposit and dissemination of scientific research documents, whether they are published or not. The documents may come from teaching and research institutions in France or abroad, or from public or private research centers.

L'archive ouverte pluridisciplinaire **HAL**, est destinée au dépôt et à la diffusion de documents scientifiques de niveau recherche, publiés ou non, émanant des établissements d'enseignement et de recherche français ou étrangers, des laboratoires publics ou privés.



Distributed under a Creative Commons Attribution - NonCommercial 4.0 International License

1 **Palaeoenvironmental changes after the Messinian Salinity Crisis in the Mediterranean**
2 **Almería-Níjar Basin (SE Spain) recorded by benthic foraminifera**

3

4 José N. Pérez-Asensio^{a,*}, Francisco J. Rodríguez-Tovar^b, Weronika Łaska^c, Alfred Uchman^c

5

6 **Authors' addresses:**

7 ^a*CEREGE UM34, Aix Marseille Univ., CNRS, IRD, INRAE, Coll France, 13545 Aix-en-
8 Provence, France*

9 ^b*Departamento de Estratigrafía y Paleontología, Facultad de Ciencias, Universidad de
10 Granada, Campus de Fuentenueva s/n, Granada, 18002, Spain*

11 ^c*Jagiellonian University, Faculty of Geography and Geology, Institute of Geological
12 Sciences, Gronostajowa 3a, 30-387 Kraków, Poland*

13

14 *corresponding author

15

16 *E-mail addresses:*

17 Corresponding author, perez@cerege.fr (J.N. Pérez-Asensio)

18 Co-authors; fjrtovar@ugr.es (F.J. Rodríguez-Tovar), weronika.laska@doctoral.uj.edu.pl (W.
19 Łaska), alfred.uchman@uj.edu.pl (A. Uchman)

20

21 **Abstract**

22 In this study, the early Pliocene palaeoenvironmental context of the Mediterranean
23 Almería-Níjar Basin (SE Spain) is analysed using benthic foraminifera, with special focus on
24 environmental conditions after the Messinian Salinity Crisis (MSC). A deep upper-slope
25 setting (274 m water depth), with high oxygen levels and low organic matter fluxes, is

26 inferred for the earliest Pliocene sediments over the Miocene-Pliocene boundary. In this
27 setting, the westernmost and earliest recolonization of the species *Siphonina reticulata* across
28 the Mediterranean is reported. This finding, along with the presence of intensively
29 bioturbated sediments and highly diverse benthic foraminiferal assemblages at —or just
30 above— the Miocene-Pliocene boundary might indicate the earliest establishment of well-
31 ventilated fully marine conditions in the Mediterranean after the MSC. Subsequent
32 shallowing from 274 to 220 m water depth during the earliest Pliocene is likely related to a
33 global sea-level drop. Palaeobathymetry remains stable around 220–230 m water depth after
34 this sea-level fall. However, three successive palaeoenvironmental subintervals could be
35 defined within this upper slope setting. Increasing continental organic matter and sediment
36 inputs indicate higher fluvial discharge during the first subinterval. The second subinterval
37 records a decrease in both terrestrial organic matter and sediment supply due to lower riverine
38 discharge. Finally, reduced input of continental organic matter suggests low river runoff
39 during the third subinterval, in which a slight increase in transported shelf foraminiferal taxa
40 may be related to vertical tectonic movements of the basin margins.

41

42 **Keywords:** Micropalaeontology; Palaeobathymetry; Organic matter; Sediment supply;
43 Riverine discharge; Pliocene

44

45 **1. Introduction**

46 The Messinian Salinity Crisis (MSC) in the Mediterranean Sea (5.97–5.33 Ma, late
47 Miocene) was one of the most dramatic palaeoenvironmental changes in the Earth's recent
48 history (Hsü et al., 1973; Roveri et al., 2014). During the MSC, the water-mass exchange
49 between the Atlantic Ocean and the Mediterranean Sea was reduced by a combination of
50 tectonic uplift and glacioeustatic sea-level fall (e.g., Weijermars, 1988; Manzi et al., 2013;

51 Pérez-Asensio et al., 2013; Flecker et al., 2015). These restricted conditions led to the
52 deposition of a giant volume of salt in the whole Mediterranean basin and subsequent
53 brackish-water conditions (Roveri et al., 2014). The processes finalizing the MSC remain
54 controversial, despite arduous scientific discussions. Three hypotheses have been proposed.
55 The first one posits a catastrophic reflooding at the beginning of the Pliocene through the
56 Strait of Gibraltar, rapidly filling the entire Mediterranean basin (Garcia-Castellanos et al.,
57 2009, 2020; Roveri et al., 2014; Caruso et al., 2020). The second invokes two-step reflooding
58 during the late Messinian-earliest Pliocene (Bache et al., 2012; Pérez-Asensio et al., 2013).
59 The third one proposes a high-water level during the Messinian in the whole Mediterranean,
60 with a minor sea-level rise (tens to few hundreds of metres) at the Miocene-Pliocene
61 boundary (Stoica et al., 2016; Andreetto et al., 2021).

62 In order to shed light on the palaeoenvironmental conditions after the MSC, it is
63 essential to analyse sedimentary records from the earliest Pliocene over the Miocene-Pliocene
64 boundary. The studied stratigraphic section (Los Ranchos) encompasses the Miocene-
65 Pliocene boundary, and includes sediments from the early Pliocene (Figs. 1 and 2). The Los
66 Ranchos section is located in the Almería-Níjar Basin, which was in the westernmost part of
67 the Mediterranean Sea during the late Miocene and early Pliocene. Therefore, the studied
68 section's sediments could record the initial arrival of Atlantic waters into the Mediterranean
69 after the MSC.

70 The main aims of this study are: 1) to obtain a detailed interpretation of the
71 palaeoenvironmental conditions after the MSC (earliest Pliocene), and 2) to analyse
72 palaeoenvironmental changes in the studied section during the early Pliocene. For these
73 purposes, benthic foraminiferal assemblages were analysed as a key proxy to interpret
74 changes in environmental conditions affecting benthic habitat such as water depth, organic

75 matter fluxes and oxygen content (Morigi et al., 2001, 2005; Jorissen et al., 2007; Drinia et
76 al., 2008; Setoyama et al., 2011; Buosi et al., 2020).

77

78 **2. Geological setting**

79 The Almería-Níjar Basin is a post-orogenic intermontane basin of the Betic Cordillera
80 (Aguirre, 1998; Yesares-García and Aguirre, 2004) (Fig. 1). This basin is limited by the Betic
81 Cordillera's basement of the Sierra Alhamilla and the Sierra de Cabrera to the N, and the
82 Sierra de Gádor mountain ranges to the W. The Neogene volcanic complex of the Sierra de
83 Gata limits the basin to the E. The sedimentary filling of the basin consists of several units,
84 separated by unconformities, ranging from the Miocene to the Pleistocene (e.g., Goy and
85 Zazo, 1986; Montenat et al., 1990; Aguirre, 1998; Yesares-García and Aguirre, 2004). Upon
86 the Betic Cordillera's metamorphic basement and the volcanic rocks of the Sierra de Gata,
87 middle Miocene conglomerates and calcilutites were deposited (Serrano, 1990). These
88 deposits are overlain by upper Miocene and Pliocene marine and continental deposits
89 (Montenat et al., 1990; Jiménez and Braga, 1993; Aguirre, 1998). The upper Miocene
90 deposits consist of marine marls, which are unconformably overlain by two Pliocene units
91 (Units I and II). The first comprises mixed siliciclastic-carbonate sediments deposited in a
92 deltaic system, and in a variety of shelf environments (Aguirre, 1998; Yesares-García and
93 Aguirre, 2004). This unit is early to middle Pliocene in age (Aguirre, 1998). Unit I was
94 deposited in a SW-NE elongated gulf open to the Mediterranean Sea to the S (Aguirre, 1998;
95 Braga et al., 2003; Martín et al., 2003). The second unit unconformably overlies Unit I and is
96 late Pliocene in age (Aguirre, 1998). It consists of siliciclastic sediments and temperate coral
97 banks of *Cladocora caespitosa* (Linnaeus, 1767) from a restricted bay, with prograding fan
98 deltas, opened to the Mediterranean Sea toward the S (Aguirre and Jiménez, 1997, 1998;
99 Aguirre, 1998; Pérez-Asensio and Aguirre, 2010). The sedimentary filling of the basin ends

100 with Quaternary deposits of sands and conglomerates deposited in alluvial fans and beach
101 environments (Goy and Zazo, 1986; Aguirre, 1998).

102

103 **3. Materials and methods**

104 The studied Los Ranchos section (GPS coordinates 37°00.351'N, 01°97.675'W) is
105 located in the northeastern area of the Almería-Níjar Basin (SE Spain), near the village of El
106 Argamasón (Fig 1). This section pertains to the early-middle Pliocene Unit I (Aguirre, 1998;
107 Yesares-García and Aguirre, 2004). The 66-m thick Los Ranchos section begins with 1 m of
108 marls (Fig. 2). They are overlain by 50 m of silts and sands. The boundary between the basal
109 marls and the silty-sandy units is intensively bioturbated with firmground *Thalassinoides* isp.
110 descending up to 60 cm from the contact. Its densely packed tunnels are filled with sandstone
111 piped from the overlying unit. The upper part of the section mostly consists of calcarenites-
112 calcirudites (14.5 m) with a thin (0.5 m) layer of silts and sands at the topmost part.

113 A total of 34 samples of 25–50 g was collected along the first 39 m of the Los
114 Ranchos section (Fig. 2) in order to reconstruct the palaeoenvironmental conditions after the
115 MSC (earliest Pliocene). These samples were wet-sieved over a 63 µm mesh. The sand
116 content was calculated as the percentage of the > 63 µm fraction. Samples were dry-sieved
117 over a 125 µm mesh for micropalaeontological analyses. A qualitative biostratigraphic dating
118 was performed based on absence/presence of planktic foraminiferal biomarkers. At least 300
119 benthic foraminifera were identified to the species level in each sample. Taxonomic
120 identifications were made using AGIP Mineraria (1982), Loeblich and Tappan (1987), Corbí
121 (2010), and Milker and Schmiedl (2012). The percentage of transported shelf taxa, which
122 included abraded and broken shells of *Ammonia* spp. (Bruennich, 1772), *Asterigerinata* spp.
123 (Bermudez, 1949), *Elphidium* spp. (de Montfort, 1808), *Haynesina* spp. (Banner and Culver,
124 1978) and *Rosalina* spp. (d'Orbigny, 1826), was calculated (Pérez-Muñoz et al., 2001; Pérez-

125 Asensio and Aguirre, 2010; Pérez-Asensio and Rodríguez-Ramírez, 2020). These
126 allochthonous species were removed from the benthic foraminiferal raw counts, and
127 discarded for palaeoenvironmental and palaeobathymetric analyses. Benthic foraminifera
128 were classified into epifaunal and infaunal microhabitats to infer changes in organic matter
129 flux to the seafloor and/or oxygen content at bottom waters (Jorissen et al., 1995, 2007). In
130 order to determine benthic foraminiferal assemblages, Q-mode principal component analysis
131 (PCA) was applied using the software OriginPro 2020. For the PCA analysis, only species
132 representing $\geq 1\%$ of the total assemblage in at least three samples were considered. Relative
133 abundances (%) of dominant species obtained with the PCA were calculated. Benthic
134 foraminiferal assemblage diversity was assessed using the Shannon-Wiener index (H) (Hill,
135 1973). Quantitative palaeobathymetry was estimated by means of the Hohenegger (2005)
136 transfer equation, removing abundant infaunal species prior to its application (Pérez-Asensio,
137 2021). Abundant infaunal species whose increase gives unrealistically deep
138 palaeobathymetric estimates were likewise removed (Pérez-Asensio, 2021). The
139 planktic/benthic ratio (P/B ratio hereafter), scored as $[P/(P+B)] \times 100$, was also calculated.
140

141 **4. Results**

142 *4.1. Planktic foraminiferal biostratigraphy*

143 The presence of planktic foraminiferal biomarkers along the studied interval is
144 depicted in Figure 3. The planktic foraminifera *Globorotalia conomiozea* (Kennett, 1966) and
145 *G. margaritae* (Bolli and Bermudez 1965) were found in the lowermost sample (R1)
146 collected in the basal marls near the boundary with the overlaying silts and sands (Figs. 3 and
147 4). The co-occurrence of both species coincides with highly bioturbated sediments. *G.*
148 *margaritae* appears in most of the samples from the silts and sands over the basal marls; its
149 presence is scarcer from ca. 20 m to the top of the studied interval (Fig. 3).

150

151 4.2. Sand content and planktic/benthic ratio

152 The sand content increases from 60% to 90% from the base of the section until ca.
153 11.5 m (Fig. 5). The middle-upper part of the section (11.5–39 m) shows stable values for
154 sand content, around 90%. The highest value for the P/B ratio (ca. 80%) is found from the
155 base to 11.5 m above. Its value gradually decreases until 23 m, to a minimum of 20%.
156 Finally, the P/B ratio has a fluctuating trend with low average values (35%) from 23 m to the
157 top of the studied interval.

158

159 4.3. Benthic foraminiferal data

160 The first sample (R1), collected within intensively bioturbated sediments, was not
161 considered for benthic foraminiferal analyses because bioturbation produces vertical mixing
162 and homogenization of benthic foraminiferal assemblages, implying misleading
163 palaeoenvironmental interpretations (Pérez-Asensio et al., 2017).

164 A total of 117 benthic foraminiferal species were identified in this study. The Q-mode
165 Principal Component Analysis (PCA) allows two assemblages to be distinguished (PC 1, PC
166 2), which respectively explain 94% and 3% of the total variance (Table 1). Benthic
167 foraminiferal assemblage PC 1, dominated by *Cibicides refulgens* (de Montfort, 1808)
168 includes *Cibicides* spp. (de Montfort, 1808), *C. lobatulus* (Walker and Jacob, 1798), *C.*
169 *mundulus* (Brady, Parker and Jones, 1888), and *Bolivina spathulata* (Williamson, 1858) as
170 secondary taxa (Fig. 4, Table 1). This assemblage dominates throughout the studied interval
171 (Fig. 5). The second assemblage (PC 2) is dominated by *Cibicidoides mundulus*, and includes
172 *Planulina ariminensis* (d'Orbigny, 1826), *Siphonina reticulata* (Czjzek, 1848), *Uvigerina*
173 *striatissima* (Perconig, 1955), *Lenticulina* spp. (Lamarck, 1804), and *Melonis pompilioides*
174 (Fichtel and Moll, 1798) as associated taxa (Fig. 4, Table 1). This second assemblage is more

175 significant in the lowermost part of the studied interval (0–4 m) (Fig. 5). The Shannon-
176 Wiener index (H) shows an upward decreasing trend with the highest average values at the
177 base of the section (~2.6) and lower average values at the top (~1.9) (Fig. 5).

178 The relative abundances (%) of the dominant and additional taxa from the Q-mode
179 PCA assemblages are plotted in Figure 6. *Cibicidoides mundulus*, *Planulina ariminensis*,
180 *Siphonina reticulata*, and *Uvigerina striatissima* show their highest abundances in the
181 lowermost part of the section (0–4 m). The highest values of *Melonis pompilioides* and
182 *Lenticulina* spp. are found in the lower part of the section (0–10 m). *Bolivina spathulata*
183 increases from the base of the studied interval to 12 m, and slightly decreases towards the top
184 of the studied interval. *Cibicidoides lobatulus* increases gradually from the base to around 28
185 m, and shows lower values in the uppermost part of the studied interval (28–39 m). *Cibicides*
186 *refulgens* has progressively increasing abundances towards the top, reaching the highest
187 values in the uppermost part (28–39 m). *Cibicides* spp. increases towards the middle part of
188 the studied interval (20 m), and slightly diminishes towards the top.

189 The percentage of infaunal benthic foraminifera is low (~16%) in the lowermost part
190 (0–4 m), and increases from the base until around 10 m, where the highest values are
191 recorded (25.4%) (Fig. 5). Then it decreases until 23 m, and remains with low average values
192 (9%) until the top. The transported shelf taxa have low values (~9%) in the lowermost part
193 (0–4 m) (Fig. 5). They increase until 10 m, reaching their highest values (40%). Values
194 decrease until around 23 m and slightly increase to the top.

195 The quantitative palaeobathymetric estimations give the highest values in the
196 lowermost part of the studied interval (0–4 m), with average values of 274 m (Fig. 7).
197 Afterwards they decrease, keeping stable values around 220 m water depth, from 4 to 23 m.
198 A very small increase in average values (230 m) is estimated for the upper part (23–39 m).

199

200 **5. Discussion**

201 *5.1. Biostratigraphic dating*

202 In the sample collected in the basal marls, the presence of *Globorotalia conomiozea*
203 (Fig. 3), belonging to the *G. miotumida* group, indicates a Messinian age (Sierro, 1985;
204 Hilgen et al., 2000; Lirer et al., 2019). *G. conomiozea* disappeared at 6.50 Ma in the
205 Mediterranean basin, well below the Miocene-Pliocene boundary (Hilgen et al., 2000). Since
206 sample R1 in the basal marls is placed just below the Miocene-Pliocene boundary, this
207 species could be reworked from lower Messinian sediments into the upper Messinian basal
208 marls. Reworked *G. conomiozea* below the Zanclean has also been reported in the
209 continental/brackish ‘Lago Mare’ sediments of the Mediterranean Cuevas del Almanzora
210 section (Vera Basin, SE Spain) (Caruso et al., 2020). In the remaining samples collected in
211 the silts and sands, only *G. margaritae* occurs, which suggests an early Pliocene (Zanclean)
212 age (Lirer et al., 2019). The first occurrence of this species in the western Mediterranean Vera
213 Basin, nearby the Los Ranchos section, was dated at 5.328 Ma (Caruso et al., 2020). The
214 presence of *G. margaritae* at the base of the silts and sands (sample R2) suggests an age of
215 5.328 Ma or younger. The absence of *Globoconella puncticulata*, whose first occurrence is at
216 4.52 Ma in the Mediterranean basin, and the occasional occurrence of *G. margaritae*, may be
217 indicative of the MPI 1 or MPI2 biozones, the two first biozones of the Zanclean (Lirer et al.,
218 2019). A more detailed biostratigraphic study is needed to discern if biozone MPI1 is present
219 or missing in the studied section. With the current biostratigraphic data, the Miocene-
220 Pliocene boundary can be placed at the top of the basal marls (Fig. 3). The presence of the
221 early Pliocene *G. margaritae* in the Messinian marls (sample R1) (Figs. 2 and 3) can be
222 explained by bioturbational downward redistribution of its tests —as supported by intense
223 bioturbation with *Thalassinoides* isp. at the Miocene-Pliocene boundary— similarly to that of
224 microfossils (i.e., calcareous nannofossils, foraminifers) in other boundaries (e.g., Rodríguez-

225 Tovar et al., 2010; Kędzierski, et al., 2011; Alegret et al., 2015). A less frequent occurrence
226 of *G. margaritae* in the upper half of the studied interval (Fig. 3) could be related to
227 unfavourable shallow conditions for this deep-water planktic foraminiferal species (Schiebel
228 and Hemleben, 2005; Kucera, 2007; Pérez-Asensio et al., 2018). Such a context would be
229 consistent with higher sand content in this part of the studied interval (Fig. 5).

230

231 *5.2. Palaeoenvironmental conditions after the Messinian salinity crisis*

232 The early Pliocene palaeoenvironmental conditions after the Messinian salinity crisis
233 (MSC) are recorded in interval A (Figs. 8 and 9a). Previous studies based on
234 sedimentological, taphonomical and palaeontological data interpreted the silts and sands of
235 this interval as a low-energy deep outer-shelf setting (Aguirre and Yesares-García, 2003;
236 Yesares-García and Aguirre, 2004). Benthic foraminiferal data provided by the present study
237 allow for a redefinition of this general water-depth range: according to the quantitative
238 palaeo-water depth estimations based on benthic foraminifera, with application of the transfer
239 equation by Hohenegger (2005), the palaeoenvironment was an upper slope setting with an
240 average water depth of 274 m (Figs. 7 and 8). Being the deepest environment recorded
241 throughout the studied interval, it is consistent with the highest P/B ratio, and the low sand
242 content (Fig. 5).

243 The dominance of the *Cibicidoides mundulus* (PC 2) assemblage, including species that
244 inhabit deep-water slope settings such as *C. mundulus*, *Planulina ariminensis*, and *Siphonina*
245 *reticulata* (Schönfeld, 1997; Pérez-Asensio et al., 2012, 2017; Holbourn et al., 2013), also
246 supports prevailing deep-water conditions after the MSC in the Almería-Níjar Basin. The
247 relatively low abundance of infaunal benthic foraminifera suggests low organic matter fluxes
248 and high oxygenation in this upper slope setting (Jorissen et al., 1995, 2007; Aguirre et al.,
249 2020) (Fig. 5). The dominance of oligotrophic and oxic species (*C. mundulus*, *P. ariminensis*,

250 *S. reticulata*) is in accordance with low organic matter fluxes and high oxygen levels (Pérez-
251 Asensio et al., 2012, 2017; Sgarrella et al., 2012). Low downslope sediment transport is
252 inferred from low percentages of transported shelf taxa (Fig. 5). Continental sediment supply
253 might have promoted downslope sediment transport. Therefore, the low percentage of shelf
254 taxa in the upper slope could indicate scarce continental riverine discharge, implying reduced
255 sediment influx and continental organic matter input (Fig. 9a). Such a scenario is furthermore
256 consistent with the low organic matter fluxes inferred for this deep palaeoenvironment.

257 The upper slope environment of 274 m water depth at the Almería-Níjar Basin
258 (western Mediterranean) suggests deep conditions right after the Miocene-Pliocene boundary
259 (5.33 Ma), when Zanclean flooding through the Strait of Gibraltar ended the MSC (Hsü et al.,
260 1973; Garcia-Castellanos et al., 2009; Roveri et al., 2014). Benthic foraminifera from the
261 earliest Zanclean at the western Mediterranean Cuevas del Almanzora section (Vera Basin,
262 SE Spain) (Fig. 1) also indicate a deep environment of more than 250 m water depth (Caruso
263 et al., 2020). In the central and eastern Mediterranean, even deeper slope settings (up to 900
264 m water depth) have been interpreted based on benthic foraminifera (Sgarrella et al., 1997;
265 Cipollari et al., 2013; Caruso et al., 2020). Our benthic foraminiferal data, pointing to an
266 upper slope deep setting, are consistent with the three different hypotheses proposed for
267 ending the MSC, i.e. catastrophic Zanclean reflooding (Garcia-Castellanos et al., 2009;
268 Roveri et al., 2014), two-step reflooding (Bache et al., 2012; Pérez-Asensio et al., 2013), and
269 Messinian high water-level (Stoica et al., 2016; Andreetto et al., 2021).

270 After the MSC, according to the Zanclean deluge hypothesis, fully marine conditions
271 were re-established throughout the Mediterranean Sea when the Strait of Gibraltar opened
272 (Hsü et al., 1973; Garcia-Castellanos et al., 2009; Roveri et al., 2014). The distribution of the
273 oxic species *Siphonina reticulata* (Drinia et al., 2008), which disappeared at 7.17 Ma because
274 of oxygen depletion before the onset of the MSC (Kouwenhoven et al., 2003), can be used to

275 trace the definitive re-establishment of oxic normal marine conditions across the
276 Mediterranean (Caruso et al., 2020).

277 The inflow of Atlantic waters through the Strait of Gibraltar re-oxygenated
278 Mediterranean waters from the west to the east, as indicated by the eastward diachronous
279 colonization of *S. reticulata* (Caruso et al., 2020). In the Cuevas del Almanzora section of the
280 nearby Vera Basin (SE Spain) (Fig. 1), this species reappeared above the Miocene-Pliocene
281 boundary at 5.29 Ma (Caruso et al., 2020) supporting hitherto known evidence of the
282 westernmost arrival of Atlantic waters to the Mediterranean Basin. In the Los Ranchos
283 section, the maximum relative abundance of *S. reticulata* (8.8%) is recorded at the first
284 sample (R2) collected at 2 cm over the Miocene-Pliocene boundary (5.33 Ma) (Fig. 6),
285 tentatively dated at 5.328 Ma or younger under our biostratigraphic interpretation. Therefore,
286 this finding could represent the westernmost and earliest reported recolonization by *S.*
287 *reticulata* in the Mediterranean Sea to date. The intensively bioturbated layer with
288 *Thalassinoides* isp. right at the Miocene-Pliocene boundary of the Los Ranchos section (Fig.
289 2) supports well-ventilated seafloor conditions (e.g., Sarvda and Bottjer, 1989; Pierre et al.,
290 2006; Watanabe et al., 2007). Across the Mediterranean Sea, the establishment of fully
291 marine conditions occurred from 20 to 250 kyrs after the Miocene-Pliocene boundary,
292 according to previous studies (Iaccarino et al., 1999; Pierre et al., 2006; Caruso et al., 2020).
293 In the Los Ranchos section, the highly diverse benthic foraminiferal assemblages (Shannon-
294 Wiener index = 2.6) support the interpretation of well-oxygenated fully marine conditions at
295 the base of the Pliocene, which are indicated by oxic species living in normal marine
296 conditions (Fig. 5). To our knowledge, this might be the earliest evidence of fully marine
297 conditions in the entire Mediterranean, thereby marking the entrance of Atlantic marine
298 waters after the late Miocene MSC.

299

300 5.3. Early Pliocene palaeoenvironmental changes

301 The early Pliocene palaeoenvironmental changes of the studied interval in the section
302 began with an upward decrease in palaeobathymetry from 274 to 220 m within the upper
303 slope setting (Figs. 7, 8 and 9). This shallowing defines the boundary between
304 palaeoenvironmental intervals A and B1-3 (Figs. 7 and 8). The palaeobathymetry decrease is
305 also recorded by the change from the deeper *Cibicidoides mundulus* (PC 2) assemblage to the
306 shallower *Cibicides refulgens* (PC 1) assemblage (Fig. 5). The latter assemblage includes
307 species such as *C. refulgens*, *Cibicides* spp., and *Cibicidoides lobatulus*, which may inhabit
308 slope or shelf environments (Schönfeld, 2002; Villanueva-Guimerans and Canudo, 2008).
309 The upsection decrease in the P/B ratio and increase in the sand content are also consistent
310 with this shallowing (Fig. 5). The slight decrease in palaeobathymetry inferred for the studied
311 interval in the upper slope silts and sands may represent the initial phase of the long-term
312 shallowing upward trend along the Los Ranchos section (Yesares-García and Aguirre, 2004)
313 (Fig. 5). This trend ended with inner-shelf calcarenites-calcirudites that prograded over the
314 sands and silts of the outer shelf and upper slope (Yesares-García and Aguirre, 2004) (Fig. 2).
315 The global sea-level curves of Hardenbol et al. (1998) and Miller et al. (2005) show a gradual
316 sea-level drop during the earliest Pliocene (Pérez-Asensio et al., 2013) that may explain the
317 shallowing upward trend at the Los Ranchos section.

318 After the shallowing at the earliest Pliocene (A-B1 boundary), palaeobathymetry
319 remained stable around 220–230 m (Figs. 7 and 8), but the abundance of infaunal taxa and
320 percentage of transported shelf taxa point to three palaeoenvironmental subintervals (B1, B2,
321 B3) (Figs. 8 and 9). Subinterval B1 records increasing infaunal taxa and transported shallow
322 water taxa abundances (Fig. 5). As explained above, high river runoff might have supplied
323 sediment and terrestrial organic matter, fostering high organic matter fluxes to the seafloor
324 and more intensive downslope transport (Fig. 9b). Increasing abundances of *Bolivina*

325 *spathulata* (Fig. 6) are also indicative of higher fluvial outflow and terrestrial organic matter
326 supply (Duchemin et al., 2008; Schmiedl et al., 2010; Pérez-Asensio et al., 2020). A high
327 abundance of *Melonis pompilioides* (Fig. 6) likewise suggests high input of organic matter
328 (Grunert et al., 2015). The upward diversity decrease in this subinterval (Fig. 5) is related to
329 rapidly increasing opportunistic infaunal taxa abundances when organic matter reached the
330 seafloor (Jorissen et al., 1995, 2007). During deposition of subinterval B2, infaunal taxa
331 decreased gradually (Figs. 5 and 7). The epifaunal species *C. lobatulus* and *C. refulgens*,
332 inhabiting oligotrophic environments (Jorissen et al., 1995, 2007; Smeulders et al., 2014),
333 increased their abundances (Fig. 6). The transported shelf taxa also showed decreasing
334 percentages (Figs. 5 and 7). Hence, organic matter fluxes and sediment downslope transport
335 diminished, most likely due to lower riverine discharge supplying less sediment and
336 continental organic matter (Fig. 9c). Finally, deposition of subinterval B3 was characterized
337 by very low organic matter input (~9% of average infaunal taxa), pointing to low river runoff
338 (Figs. 8 and 9d), which is further supported by the highest abundance of the oligotrophic
339 species *C. refulgens* (Jorissen et al., 1995; Smeulders et al., 2014) (Fig. 6). A slight increase
340 in transported shelf taxa may indicate slightly higher downslope transport. Given that riverine
341 discharge was low, tectonic movements might have contributed to downslope transport in this
342 subinterval.

343

344 **6. Conclusions**

345 Benthic foraminiferal assemblages from the Los Ranchos section of the Almería-Níjar
346 Basin (SE Spain) allowed for detailed interpretation of the palaeoenvironmental conditions
347 after the Messinian salinity crisis (earliest Pliocene) in the western Mediterranean Sea.
348 Sediments over the Miocene-Pliocene boundary were deposited in an upper slope
349 environment of around 274 m water depth, with low organic matter fluxes and high oxygen

350 content. The highest relative abundance of the benthic foraminifer *Siphonina reticulata*
351 observed 2 cm above the Miocene-Pliocene boundary could mark the westernmost and
352 earliest recolonization of this species in the whole Mediterranean region. This evidence,
353 together with intensively bioturbated sediments and highly diverse benthic foraminiferal
354 assemblages at or just above the Miocene-Pliocene boundary, might indicate the earliest
355 establishment of well-oxygenated fully marine conditions in the Mediterranean Sea after the
356 Messinian salinity crisis.

357 After the establishment of fully marine conditions at the base of the Zanclean (early
358 Pliocene), palaeobathymetry decreased from 274 to 220 m water depth during the earliest
359 Pliocene. This shallowing is concomitant with a global sea-level fall, after which palaeo-
360 water depth stabilized at around 220–230 m. In this interval, three upper-slope
361 palaeoenvironmental subintervals, based on infaunal taxa and transported shelf taxa
362 percentages, can be characterized by: B1) enhanced riverine discharge leading to a higher
363 supply of sediment and terrestrial organic matter; B2) reduced river runoff with lower input
364 of sediment and continental organic matter; and B3) low fluvial outflow and terrestrial
365 organic matter input with slightly higher downslope transport, possibly linked to tectonics.

366

367 **Declaration of competing interest**

368 The authors of this study do not have any personal or financial interests representing a
369 conflict of interest.

370

371 **Acknowledgements**

372 We thank Alexander Dickson for his editorial handling, and two anonymous
373 reviewers for their useful comments. JNPA thanks the Research Groups RNM-190 (Junta de

374 Andalucía), GRC Geociències Marines (2017 SGR 315, Generalitat de Catalunya), and
375 Climate Research Group (CEREGE). Research by FJRT has been founded by scientific
376 Projects CGL2015-66835-P and CTM2016-75129-C3-2-R (Secretaría de Estado de I+D+I,
377 Spain), and B-RNM-072-UGR18 (FEDER Andalucía), and Research Group RNM-178 (Junta
378 de Andalucía). The Jagiellonian University in Kraków supported the studies by W.Ł. (DSC
379 funds no. DS/MND/WGiG/ ING/2018). We are grateful to Jean Louise Sanders for correcting
380 the English text.

381

382

383 **References**

- 384 AGIP Mineraria, 1982. Foraminiferi padani (Terziario e Quaternario). Atlante Iconografico e
385 Distribuzione Stratigrafica, second ed. AGIP, Milano, 52 tav.
- 386 Aguirre, J., 1998. El Plioceno del SE de la Península Ibérica (provincia de Almería). Síntesis
387 estratigráfica, sedimentaria, bioestratigráfica y paleogeográfica. Rev. Soc. Geol. Esp. 11,
388 297–315.
- 389 Aguirre, J., Jiménez, A.P., 1997. Census assemblages in hard-bot-tom coastal communities: a
390 case study from the Plio-Pleistocene Mediterranean. Palaios 12, 598–608.
391 <https://doi.org/10.2307/3515415>.
- 392 Aguirre, J., Jiménez, A.P., 1998. Fossil analogues of present-day *Cladocora caespitosa* coral
393 banks: Sedimentary setting, dwelling community, and taphonomy (Late Pliocene, W
394 Mediterranean). Coral Reefs 17, 203–213. <https://doi.org/10.1007/s003380050119>.
- 395 Aguirre, J., Yesares-García, J., 2003. Análisis tafonómico y secuencial del Plioceno inferior
396 en el sector NE de la cuenca de Almería-Níjar (SE de España). Rev. Esp. Paleontol. 18,
397 61–82.

- 398 Aguirre, J., Ocaña, O., Pérez-Asensio, J.N., Domènec, R., Martinell, J., Mayoral, E. and
399 Santos, A., 2020. Mesophotic azooxanthellate coral communities and submarine seascapes
400 during the early Pliocene in Manilva Basin (S Spain). *Coral Reefs* 39, 1739–1752.
401 <https://doi.org/10.1007/s00338-020-02000-x>.
- 402 Alegret, L., Rodríguez-Tovar, F. J., Uchman, A., 2015. How bioturbation obscured the
403 Cretaceous–Palaeogene boundary record. *Terra Nova* 27, 225–230.
404 <https://doi.org/10.1111/ter.12151>.
- 405 Andreetto, F., Matsubara, K., Beets, C.J., Fortuin, A.R., Flecker, R., Krijgsman, W., 2021. High
406 Mediterranean water-level during the Lago-Mare phase of the Messinian Salinity
407 Crisis: insights from the Sr isotope records of Spanish marginal basins (SE Spain),
408 *Palaeogeogr. Palaeoclimatol. Palaeoecol.* 562, 110139.
409 <https://doi.org/10.1016/j.palaeo.2020.110139>.
- 410 Bache, F., Popescu, S.-M., Rabineau, M., Gorini, C., Suc, J.-P., Clauzon, G., Olivet, J.-L.,
411 Rubino, J.-L., Melinte-Dobrinescu, M.C., Estrada, F., Londeix, L., Armijo, R., Meyer, B.,
412 Jolivet, L., Jouannic, G., Leroux, E., Aslanian, D., Dos Reis, A.T., Mocochain, L.,
413 Dumurdžanov, N., Zagorchev, I., Lesić, V., Tomić, D., Çağatay, M.N., Brun, J.-P.,
414 Sokoutis, D., Csato, I., Ucarkus, G., Çakir, Z., 2012. A two-step process for the reflooding
415 of the Mediterranean after the Messinian salinity crisis. *Basin Res.* 24, 125–153.
416 <https://doi.org/10.1111/j.1365-2117.2011.00521.x>.
- 417 Buosi, C., Cherchi, A., Mana, D., 2020. Benthic foraminiferal proxies of environmental
418 changes during the pre-Messinian salinity crisis of the Sinis Basin (W Sardinia,
419 Mediterranean Sea). *Mar. Micropaleontol.* 155, 101822.
420 <https://doi.org/10.1016/j.marmicro.2020.101822>.

- 421 Braga, J.C., Martín, J.M., Quesada, C., 2003. Patterns and average rates of Late Neogene–
422 Recent uplift of the Betic Cordillera, SE Spain. *Geomorphology* 50, 3–26.
423 [https://doi.org/10.1016/S0169-555X\(02\)00205-2](https://doi.org/10.1016/S0169-555X(02)00205-2).
- 424 Caruso, A., Blanc-Valleron, M.-M., Da Prato, S., Rouchy, J.M., 2020. The late Messinian
425 “Lago-Mare” event and the Zanclean Reflooding in the Mediterranean Sea: new insights
426 from the Cuevas del Almanzora section (Vera Basin, South-Eastern Spain). *Earth Sci.
427 Rev.* 200, 102993. <https://doi.org/10.1016/j.earscirev.2019.102993>.
- 428 Cipollari, P., Cosentino, D., Radeff, G., Schildgen, T.F., Faranda, C., Grossi, F., Gliozzi, E.,
429 Smedile, A., Gennari, R., Darbaş, G., Dudas, F.Ö., Gürbüz, K., Nazik, A., Echtler, H.P.,
430 2013. Easternmost Mediterranean evidence of the Zanclean flooding event and subsequent
431 surface uplift: Adana Basin, southern Turkey. In: Robertson, A.H.F., Parlak, O.,
432 Ünlügenç, U.C. (Eds.), *Geological Development of Anatolia and the Easternmost
433 Mediterranean Region*. Geological Society of London Special Publications, 372, pp. 473–
434 494.
- 435 Corbí, H. (2010). Los foraminíferos de la cuenca neógena del Bajo Segura (sureste de
436 España). *Bioestratigrafía y cambios paleoambientales en relación con la Crisis de
437 Salinidad del Mediterráneo*. PhD thesis, University of Alicante, Spain.
- 438 Drinia, H., Antonarakou, A., Kontakiotis, G., 2008. On the occurrence of early Pliocene
439 marine deposits in the Ierapetra Basin, eastern Crete, Greece. *Bulletin of Geosciences* 83
440 (1), 63–78. <https://doi.org/10.1016/j.geobios.2003.11.008>.
- 441 Duchemin, G., Jorissen, F.J., Le Loc'h, F., Andrieux-Loyer, F., Hily, C., Thouzeau, G., 2008.
442 Seasonal variability of living benthic foraminifera from the outer continental shelf of the
443 Bay of Biscay. *J. Sea Res.* 59, 297–319. <https://doi.org/10.1016/j.seares.2008.03.006>.

- 444 Flecker, R., Krijgsman, W., Capella, W., de Castro Martíns, C., Dmitrieva, E., Mayser, J.P.,
445 Marzocchi, A., Modestu, S., Ochoa, D., Simon, D., Tulbure, M., van den Berg, B., van der
446 Schee, M., de Lange, G., Ellam, R., Govers, R., Gutjahr, M., Hilgen, F., Kouwenhoven,
447 T., Lofi, J., Meijer, P., Sierro, F.J., Bachiri, N., Barhoun, N., Alami, A.C., Chacon, B.,
448 Flores, J.A., Gregory, J., Howard, J., Lunt, D., Ochoa, M., Pancost, R., Vincent, S.,
449 Yousfi, M.Z., 2015. Evolution of the Late Miocene Mediterranean-Atlantic gateways and
450 their impact on regional and global environmental change. *Earth Sci. Rev.* 150, 365–392.
451 <https://doi.org/10.1016/j.earscirev.2015.08.007>.
- 452 Garcia-Castellanos, D., Estrada, F., Jimenez-Munt, I., Gorini, C., Fernàndez, M., Verges, J.,
453 De Vicente, R., 2009. Catastrophic flood of the Mediterranean after the Messinian salinity
454 crisis. *Nature* 462, 778–781, <https://doi.org/10.1038/nature08555>.
- 455 Garcia-Castellanos, D., Micallef, A., Estrada, F., Camerlenghi, A., Ercilla, G., Periáñez, R.,
456 Abril, J.M., 2020. The Zanclean megaflood of the Mediterranean—Searching for
457 independent evidence. *Earth Sci. Rev.* 201, 103061.
458 <https://doi.org/10.1016/j.earscirev.2019.103061>.
- 459 Goy, J.L., Zazo, C., 1986. Synthesis of the quaternary in the Almería littoral neotectonics
460 activity and its morphologic features, western Betics, Spain. *Tectonophysics* 130, 259–
461 270. [https://doi.org/10.1016/0040-1951\(86\)90116-2](https://doi.org/10.1016/0040-1951(86)90116-2).
- 462 Grunert, P., Skinner, L., Hodell, D.A., Piller, W.E., 2015. A micropalaeontological
463 perspective on export productivity, oxygenation and temperature in NE Atlantic deep-
464 waters across Terminations I and II. *Global Planet. Change* 131, 174–
465 191. <https://doi.org/10.1016/j.gloplacha.2015.06.002>.
- 466 Hardenbol, J., Thierry, J., Farley, M.B., Jaquin, T., de Graciansky, P., Vail, P.R., 1998.
467 Mesozoic and Cenozoic sequence chronostratigraphic framework of European basins—

- 468 chart 2: Cenozoic sequence chronostratigraphy. In: de Graciansky, P., Hardenbol, J.,
469 Jaquin, T., Vail, P.R. (Eds.), Mesozoic and Cenozoic sequence stratigraphy of European
470 basins. SEPM Special Publication, 60.
- 471 Hilgen, F.J., Iaccarino, S., Krijgsman, W., Villa, G., Langereis, C.G., Zachariasse, W.J.,
472 2000. The Global boundary Stratotype and Point (GSSP) of the Messinian Stage
473 (Uppermost Miocene). *Episodes* 23, 1–6. <https://doi.org/10.18814/epiiugs/2000/v23i3/004>.
- 474 Hill, M.O., 1973. Diversity and evenness: a unifying notation and its consequences. *Ecology*
475 54, 427–432. <https://doi.org/10.2307/1934352>.
- 476 Hohenegger, J., 2005. Estimation of environmental paleogradient values based on
477 presence/absence data: a case study using benthic foraminifera for paleodepth estimation.
478 *Palaeogeogr. Palaeoclimatol. Palaeoecol.* 217, 115–130.
479 <http://dx.doi.org/10.1016/j.palaeo.2004.11.020>.
- 480 Holbourn, A., Henderson, A.S., MacLeod, N., 2013. *Atlas of benthic foraminifera*. Wiley-
481 Blackwell, Oxford, pp. 654.
- 482 Hsü, K., Ryan, W., Cita, M., 1973. Late Miocene desiccation of the Mediterranean. *Nature*
483 242, 240–244. <https://doi.org/10.1038/242240a0>.
- 484 Iaccarino, S., Castradori, D., Cita, M.B., Di Stefano, E., Gaboardi, S., McKenzie, J.A.,
485 Spezzaferri, S., Sprovieri, R., 1999. The Miocene-Pliocene boundary and the significance
486 of the earliest Pliocene flooding in the Mediterranean. *Mem. Soc. Geol. Ital.* 54, 109–131.
- 487 Jiménez, A.P., Braga, J.C., 1993. Occurrence and taphonomy of bivalves from the Níjar reef
488 (Messinian, late Miocene, SE Spain). *Palaeogeogr. Palaeoclimatol. Palaeoecol.* 102, 239–
489 251. [https://doi.org/10.1016/0031-0182\(93\)90069-U](https://doi.org/10.1016/0031-0182(93)90069-U).

- 490 Jorissen, F.J., de Stigter, H.C., Widmark, J.G.V., 1995. A conceptual model explaining
491 benthic foraminiferal microhabitats. Mar. Micropaleontol. 26, 3–15.
492 [https://doi.org/10.1016/0377-8398\(95\)00047-X](https://doi.org/10.1016/0377-8398(95)00047-X).
- 493 Jorissen, F.J., Fontanier, C., Ellen, T., 2007. Paleoceanographical proxies based on deep-sea
494 benthic foraminiferal assemblage characteristics. In: Hillaire-Marcel, C., De Vernal, A.
495 (Eds.), Developments in Marine Geology, Vol. 1. Elsevier, Amsterdam, pp. 263–325.
496 [https://doi.org/10.1016/S1572-5480\(07\)01012-3](https://doi.org/10.1016/S1572-5480(07)01012-3).
- 497 Kouwenhoven, T.J., Hilgen, F.J., van der Zwaan, G.J., 2003. Late Tortonian–early Messinian
498 stepwise disruption of the Mediterranean-Atlantic connections: constraints from benthic
499 foraminiferal and geochemical data. Palaeogeogr. Palaeoclimatol. Palaeoecol. 198, 303–
500 319. [https://doi.org/10.1016/S0031-0182\(03\)00472-3](https://doi.org/10.1016/S0031-0182(03)00472-3).
- 501 Kędzierski, M., Rodríguez-Tovar, F.J. and Uchman, A., 2011. Vertical displacement and
502 taphonomic filtering of nannofossils by bioturbation in the Cretaceous-Paleogene
503 boundary section at Caravaca, SE Spain. Lethaia, 44, 321–328.
504 <https://doi.org/10.1111/j.1502-3931.2010.00244.x>
- 505 Kucera, M., 2007. Planktonic foraminifera as tracers of past oceanic environments. In:
506 Hillaire-Marcel, C., De Vernal, A. (Eds.), Developments in Marine Geology, Vol. 1.
507 Elsevier, Amsterdam, pp. 213–262. [https://doi.org/10.1016/S1572-5480\(07\)01011-1](https://doi.org/10.1016/S1572-5480(07)01011-1).
- 508 Lirer, F., Foresi, L.M., Iaccarino, S.M., Salvatorini, G., Turco, E., Cosentino, C., Sierro, F.J.,
509 Caruso, A., 2019. Mediterranean Neogene planktonic foraminifer biozonation and
510 biochronology. Earth Sci. Rev. 196, 102869.
511 <https://doi.org/10.1016/j.earscirev.2019.05.013>.
- 512 Loeblich Jr., A.R., Tappan, H., 1987. Foraminiferal Genera and their Classification. 2
513 Volumes. Van Reinhold Company, New York, 1: 970 pp.; 2: 213 pp.

- 514 Manzi, V., Gennari, R., Hilgen, F., Krijgsman, W., Lugli, S., Roveri, M., Sierro, F. J., 2013.
- 515 Age refinement of the Messinian salinity crisis onset in the Mediterranean. *Terra Nova* 25,
- 516 315–322. <https://doi.org/10.1111/ter.12038>.
- 517 Martín, J.M., Braga, J.C., Betzler, C., Brachert, T., 1996. Sedimentary model and high-
- 518 frequency cyclicity in a Mediterranean, shallow-shelf, temperate-carbonate environment
- 519 (uppermost Miocene, Agua Amarga Basin, Southern Spain). *Sedimentology* 43, 263–277.
- 520 <https://doi.org/10.1046/j.1365-3091.1996.d01-4.x>.
- 521 Martín, J.M., Braga, J.C., Betzler, C., 2003. Late Neogene-Recent uplift of the Cabo de Gata
- 522 volcanic province, Almería, SE Spain. *Geomorphology* 50, 27–42. [https://doi.org/10.1016/S0169-555X\(02\)00206-4](https://doi.org/10.1016/S0169-555X(02)00206-4).
- 524 Milker, Y., Schmiedl, G., 2012. A taxonomic guide to modern benthic shelf foraminifera of
- 525 the western Mediterranean Sea. *Palaeontol. Electron.* 15 (16A), 134.
- 526 palaeo-electronica.org/content/2012-issue-2-articles/223-taxonomyforaminifera.
- 527 Miller, K.G., Kominz, M.A., Browning, J.V., Wright, J.D., Mountain, G.S., Katz, M.E.,
- 528 Sugarman, P.J., Cramer, B.S., Christie-Blick, N., Pekar, S.F., 2005. The Phanerozoic
- 529 record of global sea-level change. *Science* 310, 1293–1298. <https://doi.org/10.1126/science.1116412>.
- 531 Montenat, C., Ott d'Estevou, P., Coppier, G., 1990. Les bassins Néogènes entre Alicante et
- 532 Cartagena. *Doc. Trav. IGAL* 12– 13, 313– 368.
- 533 Morigi, C., Jorissen, F.J., Gervais, A., Guichard, S., Borsetti, A.M., 2001. Benthic
- 534 foraminiferal faunas in surface sediments off NW Africa: relationship with organic flux to
- 535 the ocean floor. *J. Foraminifer. Res.* 31, 350–368. <https://doi.org/10.2113/0310350>.

- 536 Morigi, C., Jorissen, F.J., Fraticelli, S., Horton, B.P., Principi, M., Sabbatini, A., Capotondi,
537 L., Curzi, P.V., Negri, A., 2005. Benthic foraminiferal evidence for the formation of the
538 Holocene mud-belt and bathymetrical evolution in the central Adriatic Sea. *Marine
539 Micropaleontology* 57, 25–49. <https://doi.org/10.1016/j.marmicro.2005.06.001>.
- 540 Pérez-Asensio, J.N., 2021. Quantitative palaeobathymetric reconstructions based on
541 foraminiferal proxies: a case study from the Neogene of south-west Spain. *Palaeontology*
542 64, 475–488. <https://doi.org/10.1111/pala.12538>.
- 543 Pérez-Asensio, J.N., Aguirre, J., 2010. Benthic foraminiferal assemblages in temperate coral-
544 bearing deposits from the late Pliocene. *J. Foramin. Res.* 40, 61–78.
545 <https://doi.org/10.2113/gsjfr.40.1.61>.
- 546 Pérez-Asensio, J.N., Rodríguez-Ramírez, A., 2020. Benthic foraminiferal salinity index in
547 marginal-marine environments: A case study from the Holocene Guadalquivir estuary, SW
548 Spain. *Palaeogeogr. Palaeoclimatol. Palaeoecol.* 560, 110021.
549 <https://doi.org/10.1016/j.palaeo.2020.110021>.
- 550 Pérez-Asensio, J.N., Aguirre, J., Schmiedl, G., Civis, J., 2012. Messinian paleoenvironmental
551 evolution in the lower Guadalquivir Basin (SW Spain) based on benthic foraminifera.
552 *Palaeogeogr. Palaeoclimatol. Palaeoecol.* 326–328, 135–151.
553 <https://doi.org/10.1016/j.palaeo.2012.02.014>.
- 554 Pérez-Asensio, J.N., Aguirre, J., Jiménez-Moreno, G., Schmiedl, G., Civis, J., 2013.
555 Glacioeustatic control on the origin and cessation of the Messinian salinity crisis. *Glob.
556 Planet. Chang.* 111, 1–8. <https://doi.org/10.1016/j.gloplacha.2013.08.008>.
- 557 Pérez-Asensio, J.N., Aguirre, J., Rodríguez-Tovar, F.J., 2017. The effect of bioturbation by
558 polychaetes (Opheliidae) on benthic foraminiferal assemblages and test preservation.
559 *Palaeontology* 60, 807–827. <https://doi.org/10.1111/pala.12317>.

- 560 Pérez-Asensio, J.N., Larrasoña, J.C., Samankassou, E., Sierro, F.J., Garcia-Castellanos, D.,
561 Jiménez-Moreno, G., Salazar, A., Salvany, J.M., Ledesma, S., Mata, M.P., Civis, J.,
562 Mediavilla, C., 2018. Magnetobiochronology of lower Pliocene marine sediments from the
563 lower Guadalquivir Basin: Insights into the tectonic evolution of the Strait of Gibraltar
564 area. *GSA Bull.* 130, 1791–1808. <https://doi.org/10.1130/B31892.1>.
- 565 Pérez-Asensio, J.N., Frigola, J., Pena, L.D., Sierro, F.J., Reguera, M.I., Rodríguez-Tovar,
566 F.J., Dorador, J., Asioli, A., Kuhlmann, J., Huhn, K., Cacho, I., 2020. Changes in western
567 Mediterranean thermohaline circulation in association with a deglacial Organic Rich Layer
568 formation in the Alboran Sea. *Quat. Sci. Rev.* 228, 106075.
569 <https://doi.org/10.1016/j.quascirev.2019.106075>.
- 570 Pérez-Muñoz, A.B., Márquez-Crespo, R., Yesares-García, J., Sánchez-Almazo, I.M.,
571 Aguirre, J., 2001. Evolución paleoambiental durante el Plioceno inferior en la cuenca de
572 Almería-Níjar (SE de España) según las asociaciones de foraminíferos bentónicos. *Rev.*
573 *Esp. Paleontol.* 21-34.
- 574 Pierre, C., Caruso, A., Blanc-Valleron, M.-M., Rouchy, J.M., Orzsaq-Sperber, F., 2006.
575 Reconstruction of the paleoenvironmental changes around the Miocene–Pliocene
576 boundary along a West–East transect across the Mediterranean. *Sediment. Geol.* 188–189,
577 319–340. <https://doi.org/10.1016/j.sedgeo.2006.03.011>.
- 578 Rodríguez-Tovar, F.J., Uchman, A., Molina, E. and Monechi, S., 2010. Bioturbational
579 redistribution of Danian calcareous nannofossils in the uppermost Maastrichtian across the
580 K-Pg boundary at Bidart, SW France. *Geobios*, 43, 569–579.
581 <https://doi.org/10.1016/j.geobios.2010.03.002>.
- 582 Roveri, M., Flecker, R., Krijgsman, W., Lofi, J., Lugli, S., Manzi, V., Sierro, F.J., Bertini, A.,
583 Camerlenghi, A., De Lange, G.J., Govers, R., Hilgen, F.J., Hübscher, C., Meijer, P.T.,

- 584 Stoica, M., 2014. The Messinian Salinity Crisis: past and future of a great challenge for
585 marine sciences. *Mar. Geol.* 352, 25–58. <https://doi.org/10.1016/j.margeo.2014.02.002>.
- 586 Savrda, C.E., Bottjer, D.J., 1989. Trace-fossil model for reconstructing oxygenation histories
587 of ancient marine bottom waters: application to Upper Cretaceous Niobrara Formation,
588 Colorado. *Palaeogeogr. Palaeoclimatol. Palaeoecol.* 74, 49–74.
589 [https://doi.org/10.1016/0031-0182\(89\)90019-9](https://doi.org/10.1016/0031-0182(89)90019-9).
- 590 Schiebel, R., Hemleben, C., 2005. Extant planktic foraminifera: A brief review. *Palaeontol Z.*
591 79, 135–148, <https://doi.org/10.1007/BF03021758>.
- 592 Schönfeld, J., 1997. The impact of the Mediterranean Outflow Water (MOW) on Benthic
593 foraminiferal assemblages and surface sediments at the southern Portuguese continental
594 margin. *Marine Micropaleontology* 29, 211–236. [https://doi.org/10.1016/S0377-8398\(96\)00050-3](https://doi.org/10.1016/S0377-8398(96)00050-3).
- 596 Schönfeld, J., 2002. Recent benthic foraminiferal assemblages in deep high-energy
597 environments from the Gulf of Cadiz (Spain). *Mar. Micropaleontol.* 44, 141–162.
598 [https://doi.org/10.1016/S0377-8398\(01\)00039-1](https://doi.org/10.1016/S0377-8398(01)00039-1).
- 599 Schmiedl, G., Kuhnt, T., Ehrmann, W., Emeis, K.-C., Hamann, Y., Kotthoff, U., Dulski, P.,
600 Pross, J., 2010. Climatic forcing of eastern Mediterranean deep-water and benthic
601 ecosystems during the past 22 000 years. *Quat. Sci. Rev.* 29, 3006–3020.
602 <https://doi.org/10.1016/j.quascirev.2010.07.002>.
- 603 Serrano, F., 1990. El Mioceno en el área de Níjar (Almería, España). *Rev. Soc. Geol. Esp.* 3,
604 65–76.
- 605 Setoyama, E., Kaminski, M.A., Tyszka, J., 2011. The Late Cretaceous–Early Paleocene
606 palaeobathymetric trends in the southwestern Barents Sea — palaeoenvironmental

- 607 implications of benthic foraminiferal assemblage analysis. *Palaeogeogr. Palaeoclimatol.*
608 *Palaeoecol.* 307, 44–58. <https://doi.org/10.1016/j.palaeo.2011.04.021>.
- 609 Sgarrella, F., Sprovieri, R., Di Stefano, E., Caruso, A., 1997. Paleoceanographic conditions at
610 the base of the Pliocene in the Southern Mediterranean Basin. *Riv. Ital. Paleont. Strat.* 103,
611 207–220. <https://doi.org/10.13130/2039-4942/5291>.
- 612 Sgarrella, F., Di Donato, V., Sprovieri, R., 2012. Benthic foraminiferal assemblage turn-over
613 during intensification of the Northern Hemisphere glaciation in the Piacenzian Punta
614 Piccola section (Southern Italy). *Palaeogeogr. Palaeoclimatol. Palaeoecol.* 333-334, 59–
615 74. <https://doi.org/10.1016/j.palaeo.2012.03.009>.
- 616 Sierro, F.J., 1985. The replacement of the “*Globorotalia menardii*” group by the
617 “*Globorotalia miotumida*” group: an aid to recognizing the Tortonian-Messinian boundary
618 in the Mediterranean and adjacent Atlantic. *Mar. Micropaleontol.* 9, 525–535.
619 [https://doi.org/10.1016/0377-8398\(85\)90016-7](https://doi.org/10.1016/0377-8398(85)90016-7).
- 620 Smeulders, G.G.B., Koho, K.A., de Stiger, H.C., Mienis, F., de Haas, H., van Weering,
621 T.C.E., 2014. Cold-water coral habitats of Rockall and porcupine Bank, NE Atlantic
622 Ocean: sedimentary facies and benthic foraminiferal assemblages. *Deep-Sea Res. II* 99,
623 270–285. <https://doi.org/10.1016/j.dsr2.2013.10.001>.
- 624 Stoica, M., Krijgsman, W., Fortuin, A., Gliozzi, E., 2016. Paratethyan ostracods in the
625 Spanish Lago-Mare: more evidence for intra-basinal exchange at high Mediterranean sea
626 level. *Palaeogeogr. Palaeoclimatol. Palaeoecol.* 441, 854–870.
627 <https://doi.org/10.1016/j.palaeo.2015.10.034>.
- 628 Watanabe, S., Tada, R., Ikehara, K., Fujine, K., Kido, Y., 2007. Sediment fabrics,
629 oxygenation history, and circulation modes of Japan Sea during the Late Quaternary.

630 Palaeogeogr. Palaeoclimatol. Palaeoecol. 247, 50–64.
631 <https://doi.org/10.1016/j.palaeo.2006.11.021>.

632 Villanueva-Guimerans, P., Canudo, I., 2008. Assemblages of recent benthic foraminifera
633 from the northeastern Gulf of Cádiz. *Geogaceta* 44, 139–142.

634 Weijermars, R., 1988. Neogene tectonics in the western Mediterranean may have caused the
635 Messinian salinity crisis and an associated glacial event. *Tectonophysics* 148, 211–219.
636 [https://doi.org/10.1016/0040-1951\(88\)90129-1](https://doi.org/10.1016/0040-1951(88)90129-1).

637 Yesares-García, J., Aguirre, J., 2004. Quantitative taphonomic analysis and taphofacies in
638 lower Pliocene temperate carbonate–siliciclastic mixed platform deposits (Almería-Níjar
639 basin, SE Spain). *Palaeogeogr. Palaeoclimatol. Palaeoecol.* 207, 83–103.
640 <http://dx.doi.org/10.1016/j.palaeo.2004.02.002>.

641

642 **Table captions**

643 **Table 1.** Results from the Q-mode principal component analysis showing two benthic
644 foraminiferal assemblages. The explained variance (%) of each principal component (PC),
645 and the dominant and additional taxa are shown.

646

647 **Figure captions**

648 **Figure 1.** Geological map showing the principal Neogene intermontane basins of southeast
649 Spain (after Martín et al., 1996). The location of the Almería-Níjar Basin and the Los
650 Ranchos section are indicated. (For interpretation of the references to colour in this figure
651 legend, the reader is referred to the web version of this article.)

652

653 **Figure 2.** Stratigraphic column of the Los Ranchos section showing the main lithologies. The
654 position of studied samples is also shown. (For interpretation of the references to colour in
655 this figure legend, the reader is referred to the web version of this article.)

656

657 **Figure 3.** Biostratigraphy of the Los Ranchos section based on the presence/absence of
658 planktic foraminiferal biomarkers. The position of studied samples is also shown.

659

660 **Figure 4.** Scanning Electron Microscope (SEM) pictures illustrating the planktic
661 foraminiferal biomarkers and some of the most abundant and dominant benthic foraminiferal
662 species in the Los Ranchos section. a) *Globorotalia margaritae*, spiral view; b) *Globorotalia*
663 *margaritae*, umbilical view; c) *Globorotalia conomiozea*, umbilical view; d) *Cibicides*
664 *refulgens*, umbilical side; e) *Cibicides refulgens*, peripheral view; f) *Cibicidoides mundulus*,
665 spiral side; g) *Cibicidoides mundulus*, peripheral view; h) *Bolivina spathulata*, lateral view; i)
666 *Biasterigerina planorbis* (transported shelf taxa), spiral side; j) *Elphidium* spp. (transported
667 shelf taxa), side view. Scale bars = 100 µm.

668

669 **Figure 5.** Sand content (%), planktic/benthic (P/B) ratio (%), Shannon-Wiener index (H), Q-
670 mode benthic foraminiferal assemblages (PC 1 and 2) loadings, transported shelf taxa (%),
671 and infaunal taxa (%). The palaeoenvironmental intervals and subintervals are indicated. (For
672 interpretation of the references to colour in this figure legend, the reader is referred to the
673 web version of this article.)

674

675 **Figure 6.** Relative abundance (%) of the dominant and secondary taxa from the Q-mode
676 benthic foraminiferal assemblages. The palaeoenvironmental intervals and subintervals are

677 indicated. (For interpretation of the references to colour in this figure legend, the reader is
678 referred to the web version of this article.)

679

680 **Figure 7.** Palaeobathymetry (m) along the studied section. The blue line shows the estimated
681 palaeobathymetry values based on Hohenegger (2005) and Pérez-Asensio (2021). The grey
682 lines represent the 95% confidence intervals. The magenta line indicates the average
683 palaeobathymetric values for the palaeoenvironmental intervals and subintervals. The
684 palaeoenvironmental intervals and subintervals are shown. (For interpretation of the
685 references to colour in this figure legend, the reader is referred to the web version of this
686 article.)

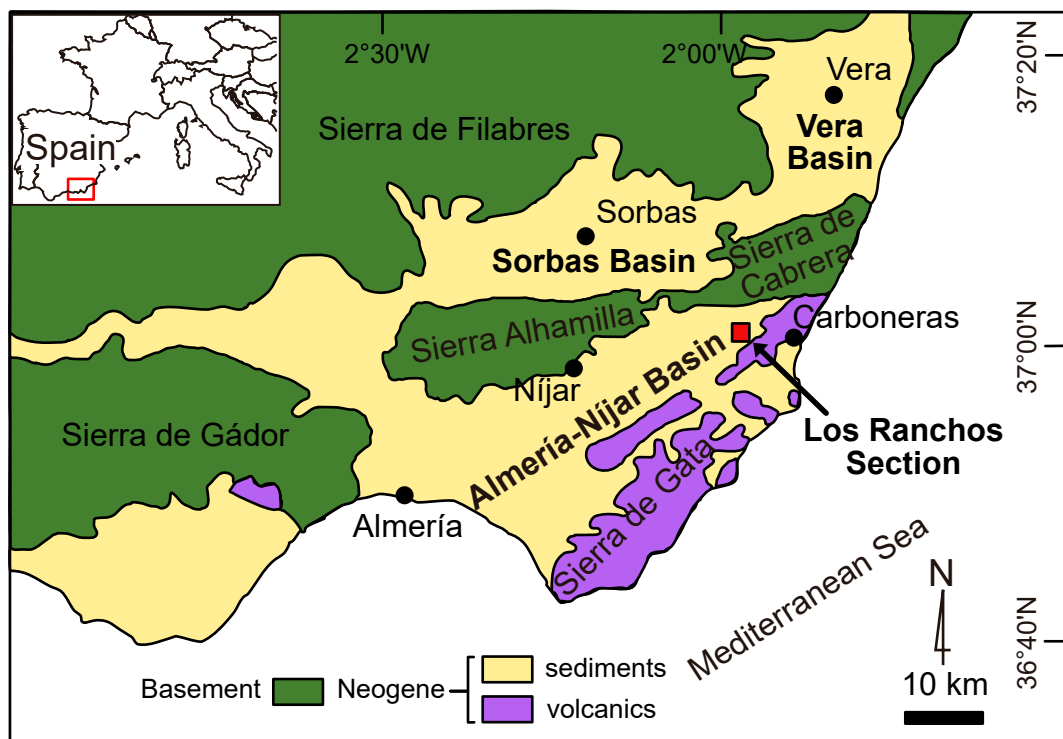
687

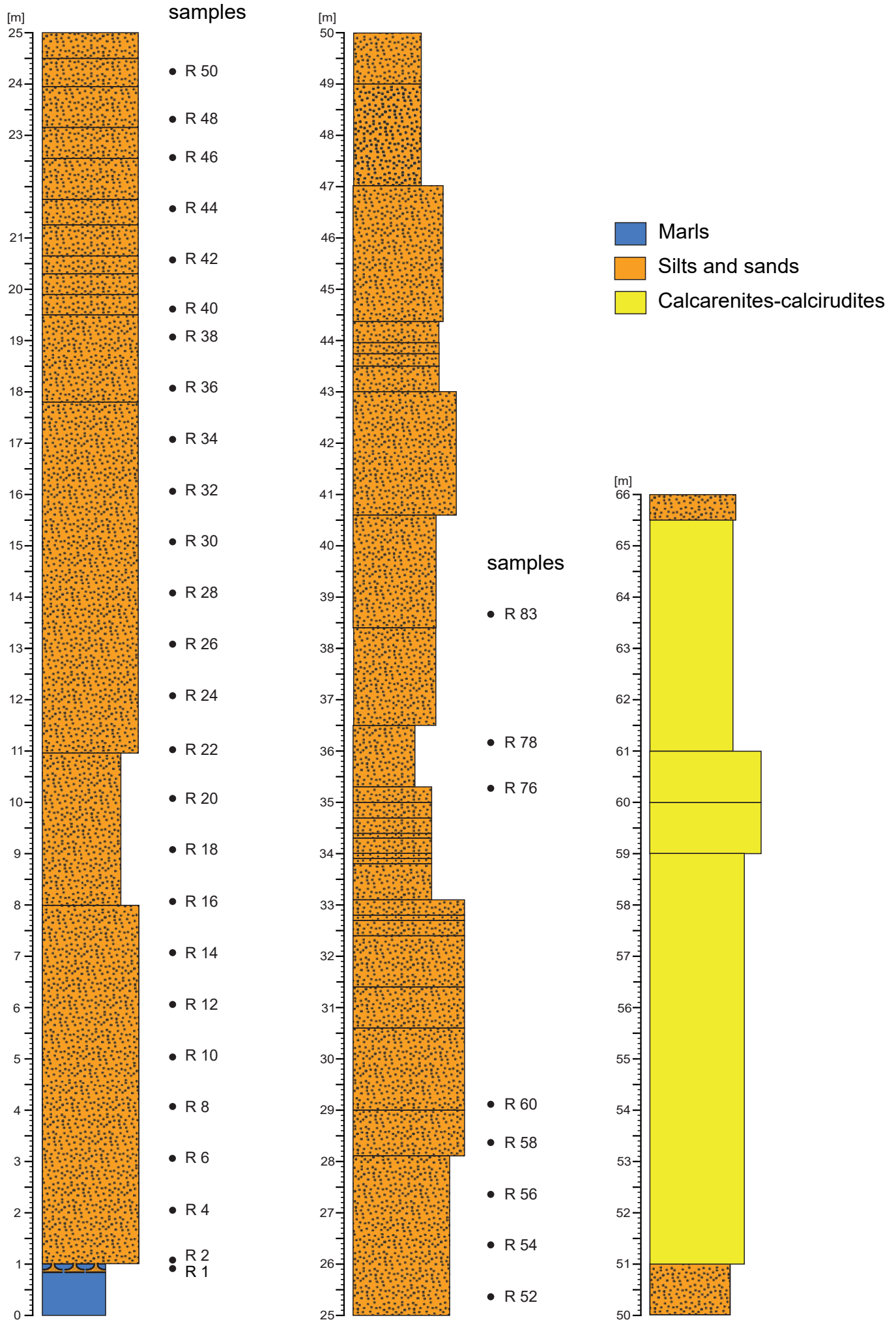
688 **Figure 8.** Palaeoenvironmental intervals and subintervals defined by water depth, organic
689 matter fluxes and shelf-taxa transport.

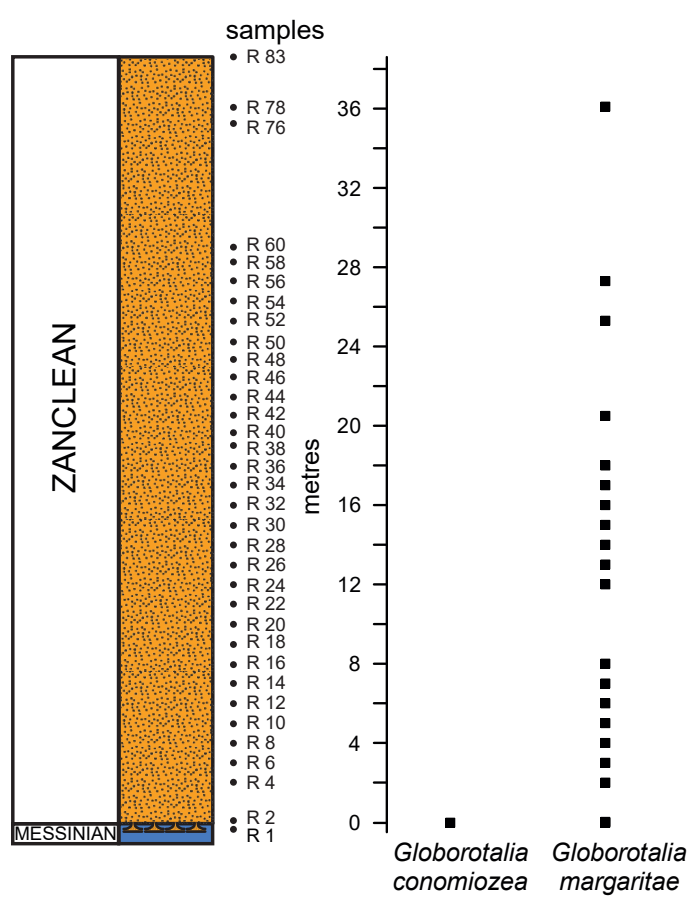
690

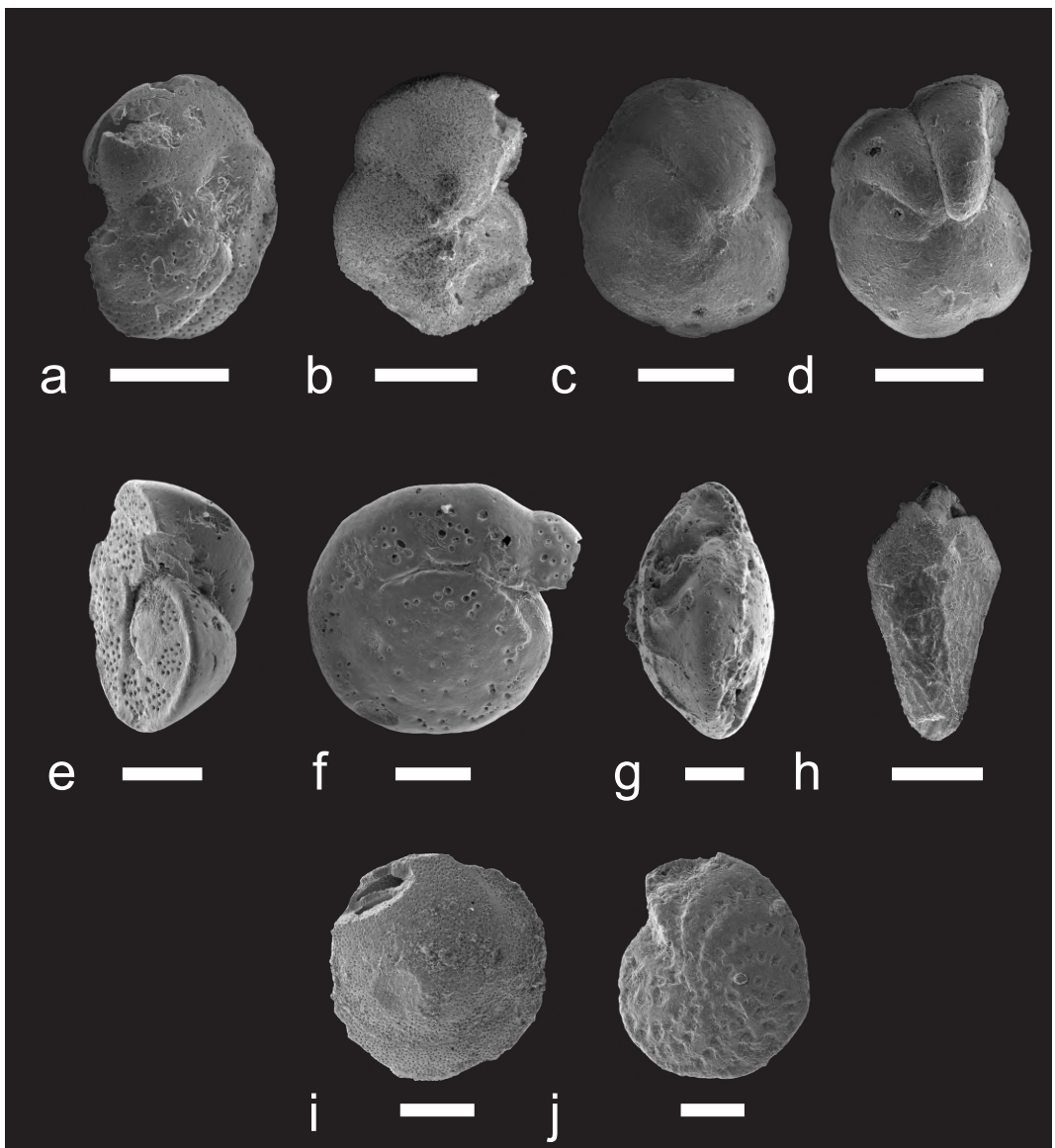
691 **Figure 9.** Simplified sketches showing the palaeoenvironmental reconstructions for the four
692 intervals and subintervals: (A) interval A, higher water depth, lower riverine discharge; (B)
693 subinterval B1, lower water depth, higher riverine discharge; (C) subinterval B2, lower water
694 depth, lower riverine discharge; (D) subinterval B3, lower water depth, lower riverine
695 discharge, tectonic movements.

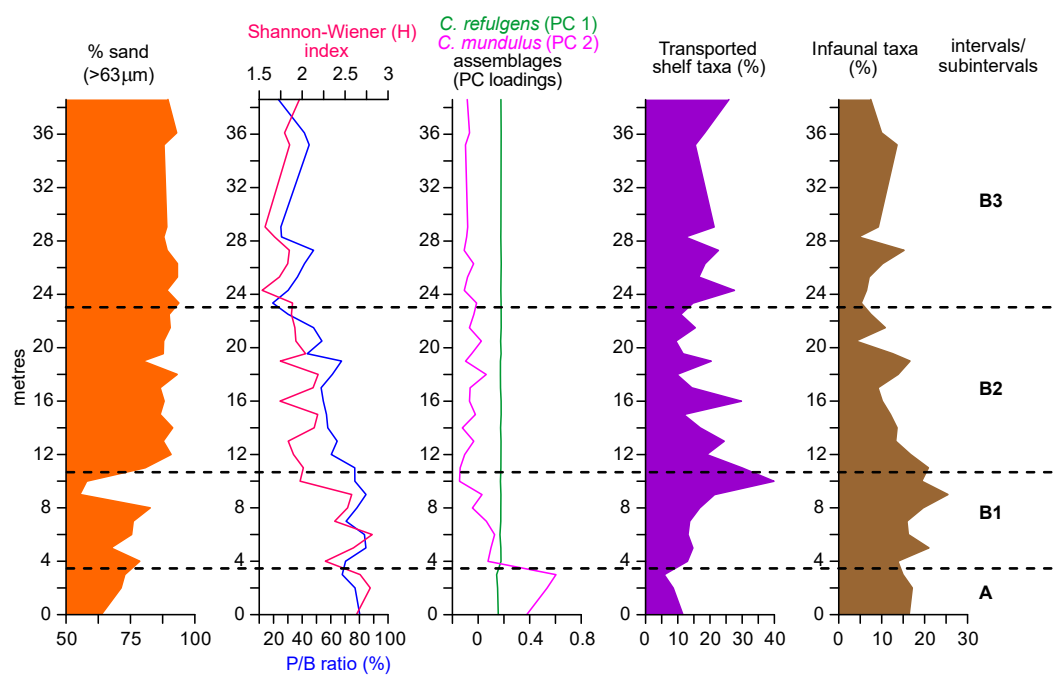
696

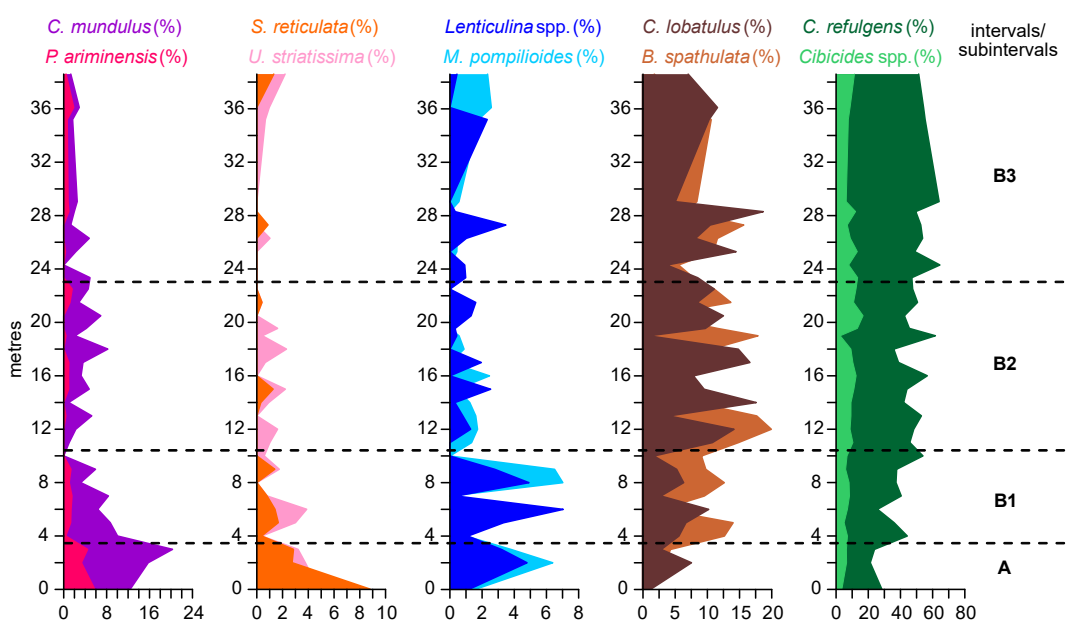


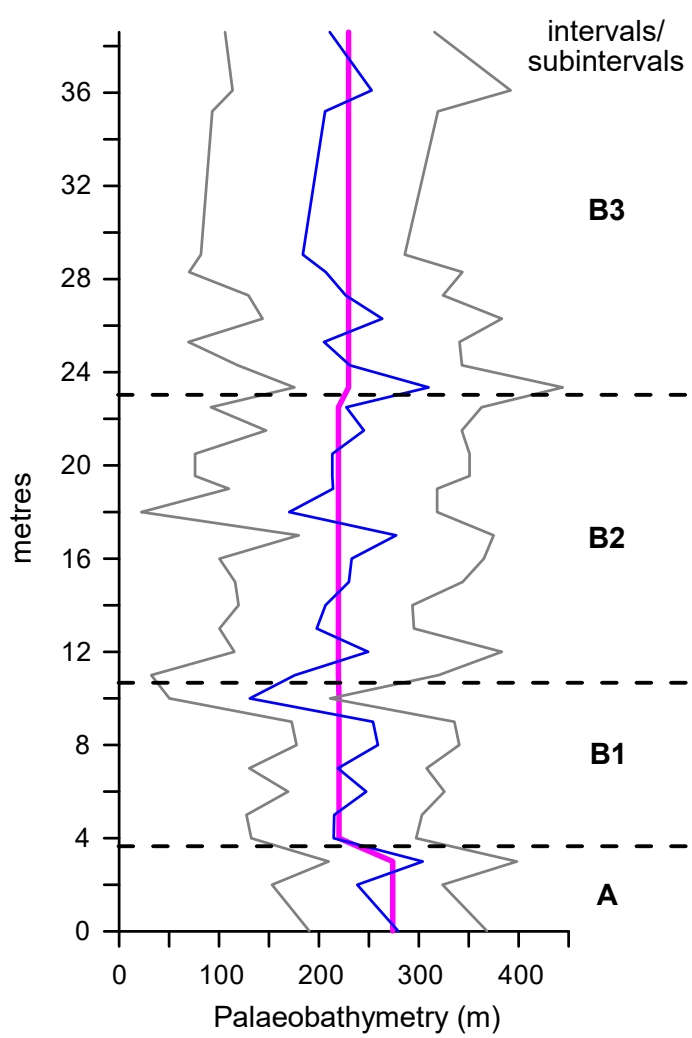


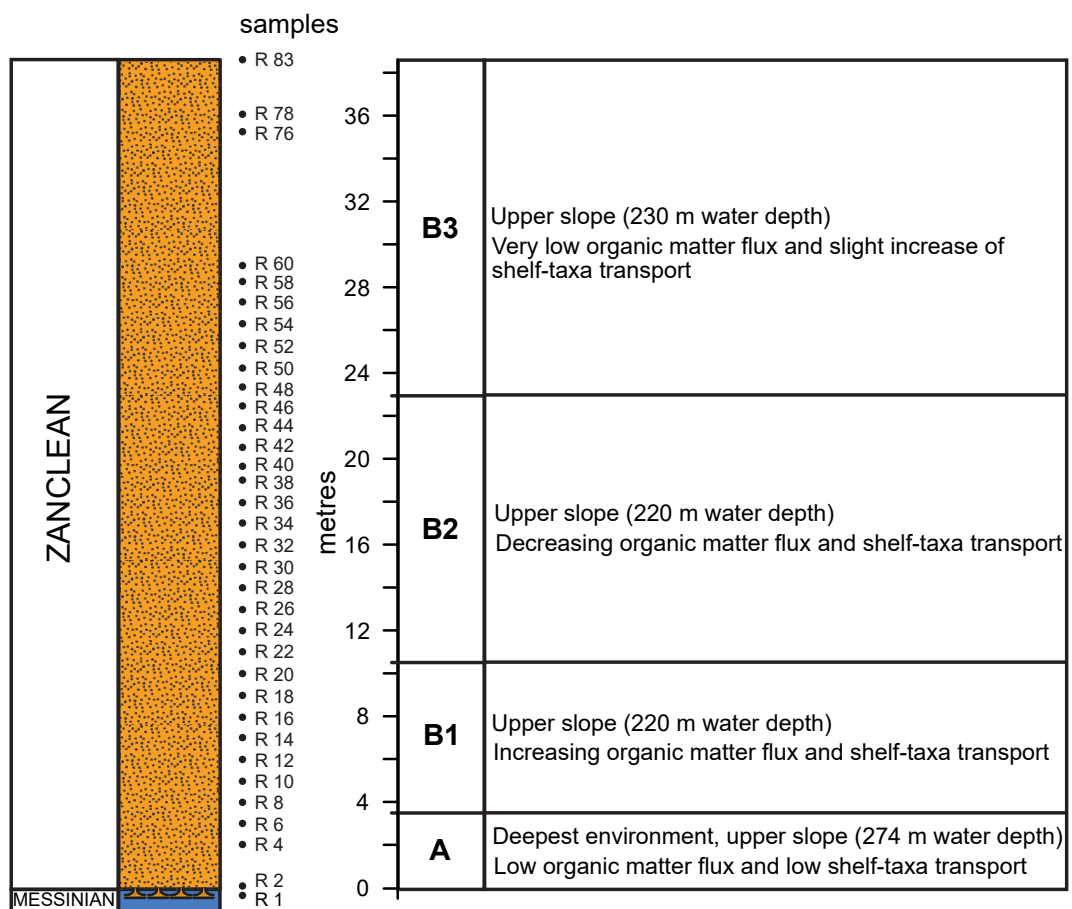












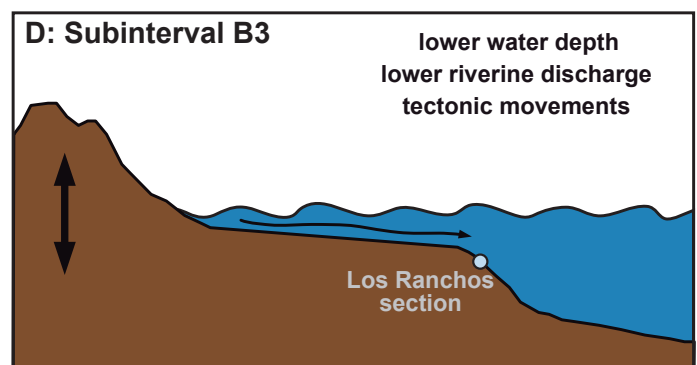
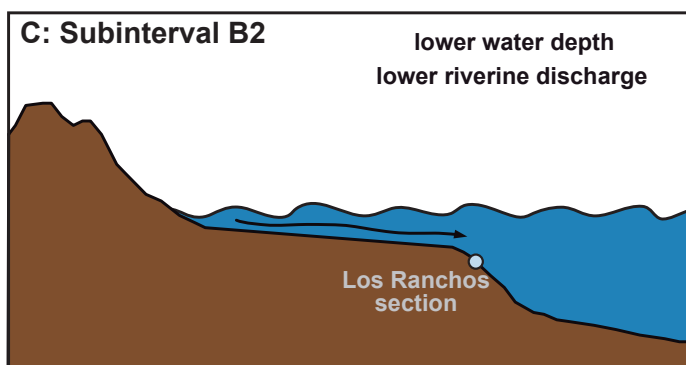
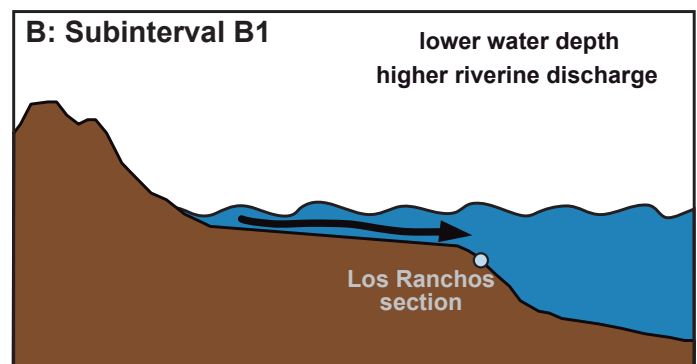
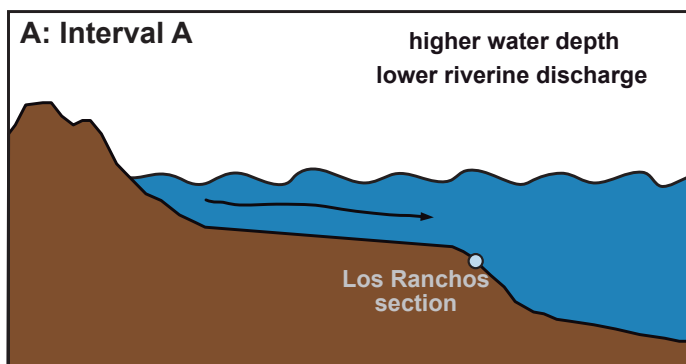


Table 1. Results from the Q-mode principal component analysis showing two benthic foraminiferal assemblages. The explained variance (%) of each principal component (PC), and the dominant and additional taxa are shown.

PC	Variance (%)	Species	Score
1	94	<i>Cibicides refulgens</i>	5.50
		<i>Cibicides</i> spp.	0.81
		<i>Cibicidoides lobatulus</i>	0.78
		<i>Cibicidoides mundulus</i>	0.37
		<i>Bolivina spathulata</i>	0.24
2	3	<i>Cibicidoides mundulus</i>	5.08
		<i>Planulina ariminensis</i>	0.88
		<i>Siphonina reticulata</i>	0.84
		<i>Uvigerina striatissima</i>	0.73
		<i>Lenticulina</i> spp.	0.61
		<i>Melonis pompilioides</i>	0.41